Ref. SCS-ES/1.2016
Issue: 1.0
Rev.: 1.0
Date: 20/03/2016

SAPIENZA UNIVERSITÀ DI ROMA

SAOCOM-CS bi-static modes for land applications
Support of Future Applications

EXECUTIVE SUMMARY

N. Pierdicca[1], M. Brogioni[5], L. Guerriero[4], R.F.Hanssen[2], L. Iannini[2], S. Paloscia[5], U. Wegmuller[3]

[1] Sapienza University of Rome. Dept. Information Engineering, Electronics, Telecommunications

[2] Delft University of Technology. Department of Geoscience and Remote Sensing

[3] Gamma Remote Sensing Research and Consulting AG

[4] University of Tor Vergata. Dipartimento di Ingegneria Civile e Ingegneria Informatica,

[5] National Research Council - IFAC

ESA/ESTEC CONTRACT n. 4000111864/14/NL/CT/

ESA STUDY CONTRACT REPORT

ESA CONTRACT N°	SUBJECT	CONTRACTOR
4000111864/14/NL/CT	**SAOCOM-CS bi-static Science for Land Applications**	Dept. Information Engineering, Electronics and Telecommunications University La Sapienza of Rome, Italy

ESA CR( ) No	STAR CODE	No of volumes : 2 This is Volume No : 1	CONTRACTOR'S REFERENCE: SCS-ES/1.2016 Issue: 1.0 Rev.: 1.0 Date: 20/03/2016

ABSTRACT :
The project summarized here was conceived to support the definition of applications, products and user requirements, as well as the hardware design and ground processing design of a companion satellite mission which will carry aboard a "passive" radar working in tandem with the Argentinian L-band radar developed by CONAE and denoted as SAOCOM. The primary objective (i.e., science driver) of the SAOCOM companion satellite mission (SAOCOM-CS) is forest tomography, which will be carried out by exploiting small baselines between active and passive systems (order of km) changing with time. Conversely, this document summarizes the investigation carried out for different bistatic radar configurations (denoted as Bistatic-1, Bistatic-2 and Specular), which are generally characterized by much larger spatial baselines (up to hundreds of km) and bistatic angles with very large components both in azimuth and in elevation. In the project the issues related to image focusing and image quality were firstly addressed. A theoretical investigation on the bistatic scattering of bare and vegetated soil provided also a general description of the scattering amplitude expected in different bistatic geometry to support the performance assessment during system design. The demonstration products (soil moisture and vegetation biomass) exploiting scattering intensity measurements were identified. The expected performances were predicted using electromagnetic models in any bistatic geometry, so that the selection of best system configurations (geometry, polarization) was finally possible. Examples of retrieval results on simulated data are also reported. Theoretical investigations were also used to predict the performances and to select the optimal baseline for interferometric applications (3-D deformation). A sketch of the InSAR data processing and multistatic InSAR product generation was given. As most of the conclusions were based on theoretical considerations, possible experimental activities to be carried out during the prosecution of mission preparation and before the launch were indicated.

The work described in this report was done under ESA Contract. Responsibility for the contents resides in the author or organisation that prepared it.

Names of authors :

M. Brogioni, L. Guerriero, R.F. Hanssen, L. Iannini, S. Paloscia, N. Pierdicca, U. Wegmuller

NAME OF ESA STUDY MANAGER	ESA BUDGET HEADING
Nicolas Floury DIV: Electromagnetics and Space Environments (EE) DIRECTORATE: TEC	060 - GSP

Acronyms and abbreviations

AIL	Action Item List
AT	Along Track
DEEI	Dept. of Electronic Engineering and Information
DICII	Dipartimento di Ingegneria Civile e Ingegneria Informatica
DIET	Dept. Information Engineering, Electronics and Telecommunications
EO	Earth Observation
ESA	European Space Agency
InSAR	SAR interferometry
LBB	Large Baseline Bistatic
MoM	Minute of Meeting
NESz	Noise Equivalent Sigma zero
PR	Progress Report
PS	Permanent Scatterer
RMS	Room Mean Square
SAP	Sapienza University of Rome
SAR	Synthetic Aperture Radar
SLC	Single Look Complex
SMC	Soil Moisture Content
SOW	Statement of Work
TN	Technical Note
XT	Across Track
WBS	Work Breakdown Structure
WP	Work Package
WV	Water Vapour

Applicable documents

AD.1	Request for Proposal IPL-PEO/CT/ct/14.705, Annex 1, 2a, 2b.
AD.2	Statement of Work. ESA Express Procurement EXPRO. SAOCOM-CS bi-static modes for land applications. Appendix 1 to RFP IPL-PEO/CT/ct/14.705. TEC-EP/2014.92/NF, Issue 1, Revision 5, Date of Issue 15/07/2014
AD.3	The General Clauses and Conditions for ESA Contracts (herein referred to as GCC), reference ESA/REG/002, REV 1.
AD.4	The Standard Requirements for Management, Reporting, Meetings and Deliverables and its Annex A: Layout for Contract Closure Documentation
AD.5	M. Brogioni, L. Guerriero, S. Paloscia, N. Pierdicca, R. Hansenn, U. Wegmuller, "SAOCOM-CS bi-static imaging, radiometry and interferometry over land", SCS-TN/01.2014, Issue 1, Rev. 1, November 24, 2014.
AD.6	M. Brogioni, L. Guerriero, S. Paloscia, N. Pierdicca, "L-band bistatic radiometry over land", SCS-TN2/1.2015, 12 May 2015.
AD.7	M. Brogioni, L. Guerriero, S. Paloscia, N. Pierdicca, "Potential SAOCOM CS land surface products - Radiometry", SCS-DP1/03.2015, 12 May 2015.

AD.8 U. Wegmüller, N. Pierdicca, "SAOCOM-CS bi-static imaging, radiometry and interferometry over land", SCS-TN1/1.2015, Issue 2, Rev. 1, 5 May 2015.

AD.9 R.F.Hanssen, L. Iannini, "L-band bi-static interferometry over land surfaces", SCS-TN3/01.2015, Issue 3, Rev. 2, 20 January 2016

AD.10 M. Brogioni, L. Guerriero, S. Paloscia, N. Pierdicca, R.F.Hanssen, L. Iannini, "Radiometry and interferometry SAOCOM-CS Lvl2 products for land surfaces", SCS-TN4/1.2016, Issue: 2.0, Rev.: 1.0, 01/03/2016.

AD.11 S. Paloscia, R. Hansenn, U. Wegmuller, M. Brogioni, L. Guerriero, N. Pierdicca, "Airborne campaign objectives and definition and preliminary campaign plan", SCS-DP5/05.2015, Issue 2.0, Rev. 1.0, 01/03/2016

AD.12 M. Brogioni, L. Guerriero, S. Paloscia, N. Pierdicca, R.F.Hanssen, L. Iannini, "Documented SAOCOM CS potential Lv2 products", SCS-DP4/1.2016, Issue 1.0, Rev. 1.0, 20/03/2016

AD.13 SAOCOM-CS Science Expert Group, "SAOCOM Companion Satellite Science Report ", ESA Reference EOP-SM/2764/MWJD-mwjd, Issue 1, Revision 2, Date of Issue 12/01/2014

Table of contents:

SCOPE

This Executive Summary summarizes the activity carried out in the frame of an ESA funded project (ESA/ESTEC CONTRACT n. 4000111864/14/NL/CT/) entitled "SAOCOM-CS bi-static modes for land applications. Support of Future Applications".

The project was intended to support the definition of applications, products and user requirements, as well as the hardware design and ground processing design of a companion satellite mission, which will carry aboard a "passive" radar working in tandem with the Argentinian L-band radar developed by CONAE and denoted as SAOCOM. The primary objective (i.e., **science driver)** of the SAOCOM companion satellite mission (SAOCOM-CS) is forest tomography, which will be carried out by exploiting small baselines between active and passive systems (order of km). Conversely, this project was devoted to the investigation of different bistatic radar configurations (denoted as Bistatic-1, Bistatic-2 and Specular), which are generally characterized by much larger spatial baselines (up to hundreds of km) and bistatic angles with very large components both in azimuth and in elevation. Demonstration products and additional experimental objectives of the SAOCOM-CS mission are investigated. The issues related to image focusing and image quality are addressed, together with possible applications exploiting either the signal phase (i.e., interferometry applications of a bistatic system) or the scattered signal amplitude (i.e., geophysical parameter estimation using the bistatic signal jointly with the monostatic SAOCOM data).

1 SCIENTIFIC MOTIVATIONS

1.1 Soil Moisture and vegetation monitoring

Soil moisture. Soil Moisture Content (SMC) is an Essential Climate Variable (ECV) considered an observational priority in the ESA's Living Planet Programme due to the multiple involvements in several environmental processes. Retrieval of this variable from space is not straightforward, since SMC variations are usually combined with simultaneous changes of other parameters, such as surface roughness, vegetation biomass, and so on. According to the present study, the synergistic use of a bistatic SAR (SAOCOM-CS) and of a monostatic one (SAOCOM) will lead to a better accuracy in SMC estimation with respect to the one expected from monostatic radar.

Vegetation Biomass. Monitoring vegetation biomass is among the most relevant applications of remote sensing in ecology and agriculture. Several studies conducted since the early 1990s with spaceborne and airborne SAR systems, as well as with theoretical models, demonstrated that L band radar signatures contain important information about crop and forest biomass. However, a saturation problem has been often observed entailing that the backscattering measurements are no longer sensitive to biomass variation after a certain amount of biomass, which depends on the electromagnetic frequency. Bistatic measurements offer the opportunity to monitor vegetation through different mechanisms with respect to the monostatic configuration, thus yielding additional information to the retrieval process.

1.2 Surface deformation

Surface deformation measurements are essential to retrieve information on geophysical processes that can be regarded as natural hazards, such as tectonics, volcanism, landslides, and ice motion. Although satellite SAR interferometry has contributed significantly in these fields, one of the main limitations is that only 1D information (in the line-of-sight of the radar) is retrieved, or in a limited number of cases 2D information by combining ascending and descending satellite passes. Thus, there is a strong need to estimate 3D deformation over wide spatial ranges. Moreover, for a fixed imaging geometry, many objects will not provide a significantly strong reflection to be used as persistent scattering, which limits the spatial sampling density over a region. SAOCOM CS will be able to provide a solution to these problems. During the mission cycles with a long along-track (AT) bistatic baseline, the combination of ascending and descending orbits will produce four measurements from different viewing geometries, enabling for the first time the estimation of the 3D motion vector. The differences in the viewing geometries will result in different independent sets of persistent scatterers, which enables us to sample the area more densely, and mitigate the saturation problem. This is of interest for several use cases: (1) to measure deformation of the earth's surface, (2) to measure deformation of objects (assets), and (3) to measure the distribution of atmospheric refractivity.

1.3 Radio science and new applications

Understanding the properties of electromagnetic wave scattering from the Earth surface in any direction, in addition to the radar illumination direction, is on its own a scientific issue. Acquiring such kind of data could provide a reference to validate electromagnetic models, to understand the involved scattering mechanisms and, especially, to pave the way to new Earth science applications, still not fully demonstrated or even not yet envisaged, that could be made possible using bistatic radar imaging. This radio science topic is also of interest in passive microwave radiometry, bistatic radar techniques for planetology and for characterizing surface clutter in "passive radar" for target reconnaissance. Provided the bistatic observation get the imprint of different scattering mechanisms, it may in principle be exploited as an independent piece of information on the target, leading to its discrimination or to the retrieval of bio-geophysical parameters. Even the temporal coherence of targets, measured from different directions in addition to the monostatic one, can bring independent information in the process of surface classification and parameter retrieval.

2 BISTATIC IMAGING

A bistatic radar operates with separated transmitting and receiving antennas. When more receivers overlap the same spatial coverage, it is referred to as a multistatic radar, so that independent observations of the same surface target can be combined to form a target state estimate. This includes the case of using a monostatic radar as transmitter and combining data from monostatic and bistatic common coverage as in the case of SAOCOM and SAOCOM-CS..

The bistatic geometry is generally described with respect to a coordinate system with the z axes being the vertical axes. The observable is the bistatic scattering coefficient σ^o_{pq},

assuming a p-polarized incident wave and a q-polarized receiver. For a bistatic imaging system, the image coordinates are the total time delay (or slant range), which is the sum of transmit and receive time delays, and the total Doppler shift, which is the sum of transmit and receive Doppler. The corresponding area on the ground is a parallelogram, instead of a rectangle as for the monostatic case. It is therefore still feasible to get an image, being the range and lateral resolutions dependent from the observation direction (zenith and azimuth scattering direction). The latter, on their turn, are determined by the along track (AT) and across track (XT) baselines that separate the active and passive platforms. A part from around specular and at very large zenith scattering angles, the resolution is only slightly reduced with respect to monostatic.

For a coherent receiver the phase is another observable in bistatic, that can be used to generate interferograms as in the case of a monostatic SAR, provided coherence is not destroyed because of temporal or spatial decorrelation.

In the direction around the specular one the range resolution is very low, so that it is only limited by the angular discrimination of the receiving antenna (about 40 km on the Earth surface), as in the case of a scatterometer, rather than by the synthetic antenna. However, as the specular signal is mainly determined by the coherent reflected component, the signal from the Earth comes mainly from the first Fresnel zone on the surface (which is the order of one km). In specular configuration SAOCOM-CS will acquire the coherent reflection along a strip parallel to the satellite track; each data sample includes several pixels of the monostatic image in the range direction. The strips can be shifted along different cycles in case there will be a continuous change in the XT baseline, thus sampling additional areas.

Depending on the modes of operation of SAOCOM-CS different approaches to focus the synthetic antenna and generate the bistatic images can be foreseen (e.g., range Doppler or time domain processing). A highly critical element for the focussing of bistatic data is the availability of adequate (phase) synchronization information between the SAOCOM transmission and the CS receiver. Furthermore, accurate information on the orbit of the two satellites is required.

For the Bistatic-1 and 2 modes two L1 bistatic products are foreseen. The first one (Level 1) is a complex valued SLC product in total range – total Doppler geometry. The second one (Level 1b) is a product in a geodetic datum. This product level shall facilitate the use of multistatic acquisitions by users without deep understanding of the bistatic SAR geometry. For the specular mode a scatterometer like monitoring of the received power may be a reasonable L1 product.

The strategy used in the assessment of the bistatic modes L1 product quality is to build upon the related assessment of the product quality for the tomographic mode data. With simple considerations the spatial resolution and NESZ results are those summarized in Table 2-1.

Table 2-1: Spatial resolution and NESZ of bistastic modes relative to tomographic mode.

Mode	Ground-range resolution	Azimuth resolution	NESZ
Tomographic	r_{tomo}	az_{tomo}	$NESZ_{tomo}$
Bistatic-1	~ r_{tomo}	~ az_{tomo}	$NESZ_{tomo}$ + 0.5dB (for B_{at} = 250 km)

Bistatic-2	$1.5r_{tomo}$ to $2.2r_{tomo}$ (for steep rec. inc. angles)	~ az_{tomo}	~ $NESZ_{tomo}$ for steep rec. inc. angle to $NESZ_{tomo}$ + 1.5dB for B_{at} = 500 km
Specular	Ambiguous for specular direction ~ 4.0 r_{tomo} at 10deg. away from specular direction)	~ az_{tomo}	~ $NESZ_{tomo}$

For the Bistatic-1 case (rel. small cross-track baseline, 0 – 250 km along track baseline) the rang ambiguity gets slightly more severe than for the quasi-monostatic case because of the slightly larger observation angle of the receive antenna used to receive the scattering from a given area on the ground. For the Bistatic-2 case (view angle differences around 90 deg.) the situation differs significantly from the quasi-monostatic and Bistatic-1 cases. For the range ambiguity not so much the elevation antenna pattern of the companion satellite, but its azimuth antenna pattern becomes relevant – and this is narrower (CS elevation pattern width is 5.45 deg. versus an azimuth pattern width of 2.0 deg.) – and consequently, range ambiguity should be less of a problem than for the quasi-monostatic case.

With increasing bistatic angles the cross-polarization will increase. At 45 deg. its level will be comparable to the like polarization scattering and at 90 deg. the cross-polarized scattering will be clearly stronger than the like polarization scattering. In Bistatic-2 mode very low scattering is expected. Therefore, having a low NESZ is very important. Noise also affects the quality of the interferometric phase. No particular problems are expected for the InSAR phase quality, but the exception may be in Bistatic-2 mode with extremely low scattering. Moreover, one precondition for the implementation of bistatic repeat-pass is that common spectral bands of the reflectivity spectrum need to be sampled by the bistatic repeat observations. This means that the reflectivity spectra of two subsequent repeat observations should overlap by about 80%. However, a drift of the AT baseline is presently not recommended for most of the interferometry applications discussed in this document later on.

The NESZ is of course not a problem for the specular configuration, where a very high scattering is generally expected. Then the receiver should be designed with high dynamic range or equipped with variable attenuator in the RF front-end.

Another issue for the bistatic modes is that the geometry (e.g., the total slant range and therefore the timing of the reception) will vary and so there will probably be times when the reflected signal from the ground (specular forward scattering) falls into the receive interval.

For the bistatic configuration using dedicated transponders can support geometric, radiometric, and phase calibration. Furthermore, it can also be used for the polarimetric calibration, assuming that the transponder can select the polarizations of the received and retransmitted signals.

3 THEORETICAL INVESTIGATIONS OF LAND BISTATIC SCATTERING

ESA demonstrated its interest in bistatic observation of land surfaces supporting a theoretical study in 2006 whose main outcome was that land surfaces present peculiar

scattering properties when the bistatic angle is large. As far as bistatic SAR devoted to land applications, the potential of this technique has been evaluated mainly by means of theoretical simulations carried out by microwave interaction models.

3.1 Bare soil

In order to progress into this issue, taking advantage from the heritage of previous work, in the present work, in addition to the Advance Integration Model (AIEM), we have made use of the Small Slope Approximation (SSA) model developed up to the 2nd order. SSA2 simulations were provided in kind courtesy by Dr. J. Johnson (Ohio State University, USA) and cover all scenarios (different soil moisture and roughness) considered in the study.

An investigation was carried out to compare the AIEM and SSA2 model simulations. The two models show a very good agreement over almost all the scattering planes, except for some directions: along the incidence plane for the cross-pol and the orthogonal plane for the co-pols. In these directions the difference is due to the mathematical formulation of AIEM which is developed at first order only. Thus the validity of previous studies can be confirmed, provided the exclusion of particular combinations of scattering angles.

The following step was the analysis of the intensity of bistatic scattering coefficient that can be encountered in the various scenarios. This task is important to support the design of the radar system (i.e., specifying the required dynamic range or the noise equivalent sigma naught, NESz), since bistatic scattering has a very wide dynamic depending, in particular, on the bistatic geometry. An example of the profile of scattering coefficient obtained at $\theta_s=\theta_i$ and $0°<\varphi_s<180°$ (scattering cone) is shown in Figure 3-1.

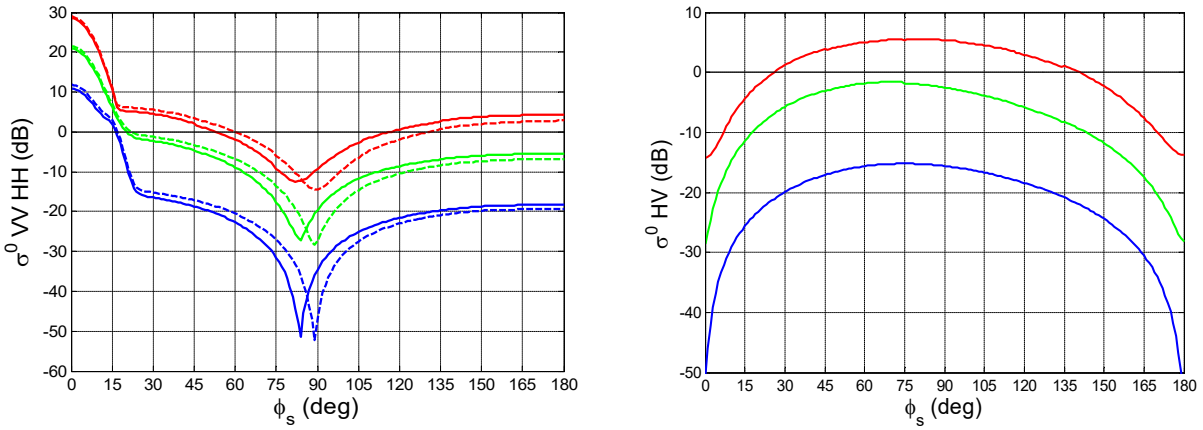

Figure 3-1: Mean (green), minimum (blue) and maximum (red) scattering coefficient for bare soil along azimuth cone with constant ϑ_s=20°. VV pol is represented on the left by continuous lines while HH pol by dashed lines.

A sensitivity analysis for soil bistatic scattering based on the model output provided a first insight in order to select those configurations of the bistatic system (polarizations and angles) which show the highest performances in SMC retrieval. Observation directions orthogonal to the incidence plane showed low values of scattering in co-polar (HH and VV) but at the same time a higher sensitivity to soil moisture with respect to backscattering. Then, in specular direction, the sensitivity to roughness was proved to be opposite to that in other bistatic directions.

3.2 Vegetated soil

The sensitivity analysis for the vegetated target has been carried out using the Tor Vergata (TOV) model for two vegetation covers: corn and a deciduous forest. The soil bistatic simulations performed by SSA2 have been included in the TOV model. In general, it is found again that the lowest co-polar scattering is met on the plane orthogonal to the incidence one (i.e. φ_s=90°), while on this same plane the highest cross-polarized scattering occurs.

The best bistatic configurations for vegetation monitoring were found when the scattering angle lies in the orthogonal plane with respect to the plane of incidence. In these configurations, the sensitivity of bistatic σ^0_{VV} at φ_s~90° is enhanced by the minimum of the soil contribution to which the double bounce mechanism is superimposed. The sensitivity of VV scattering at φ_s~ 90° is mainly determined by the interaction term which, along the forward scattering cone, is almost exclusively composed by the Double Bounce effect. In this configuration, the vegetation growth can be monitored through the changing stem height. On the contrary, in HV monostatic configuration σ^0 is determined by volume scattering, not Double Bounce, whereas in monostatic co-pol the Double Bounce is screened by surface scattering.

In forests, although the Double Bounce mechanism still occurs, trunk forward scattering is more pronounced in the backward and forward direction, rather than being almost isotropic. Moreover, it is significant when the biomass is low, while it becomes negligible when the biomass is large because of the strong trunk and crown attenuation. The signal is mainly determined by volume scattering, which tends to be isotropic as the biomass increases. We can therefore conclude that observation of forests in Bistatic-2 would add little information with respect to cross-polarized backscattering. Instead, forest can be effectively observed at specular configuration.

4 MULTISTATIC APPLICATIONS BASED ON RADAR INTENSITY

4.1 Bio-geophysical parameter retrieval: performances and L1 data requirement

The main outcome of this project was the identification of the bistatic geometry that leads to the best performances of the bio-geophysical parameter retrieval addressed before, i.e., soil moisture and vegetation biomass, taking into account the expected Level 1 product quality, especially sensitivity and noise level. To this aim, a rapid assessment of all possible bistatic configurations (e.g., bistatic angles, incidence angles, polarizations) was carried out by computing the Cramér-Rao Lower Bound (CRLB) that gives the best achievable accuracy of any unbiased estimator. An additive Gaussian error was assumed equal to 1dB, which accounts for radiometric resolution and calibration errors of the system. As far as the $NE\sigma^0$ is concerned, it is accounted for by saturating the measurements predicted by the model to the expected NESz value. Another tool used to predict the retrieval accuracy is the Chi-square, which predicts the retrieval error standard deviation in case of a linear regression estimator.

4.1.1 *Soil moisture*

The normalized CRLB (i.e., the square root of the ratio between the bistatic CRLB and the monostatic one) evaluates if a given bistatic geometrical, i.e., (θ_s, φ_s), and polarization configuration can improve the SMC retrieval with respect to monostatic measurements only. In order to limit the possibility of measurements performed below the NESz, we considered here an incidence angle of 20°, which exhibits higher scattering intensity. From now on, the idea is that we "add" bistatic data to a monostatic system (i.e., the reference) and we evaluate the improvement.

Figure 4-1 provides an example of the use of CRLB maps to identify the best scattering direction to retrieve soil moisture when soil roughness acts as a nuisance parameter (i.e., a noisy unknown term in the retrieval). It shows that the use of bistatic VV polarization can be useful when the measurement is performed in forward directions, i.e., azimuth scattering angles φ_s<90°. In particular, the improvement is higher around the orthogonal plane, on the sides of the VV pol minimum scattering at high zenith angles. If we consider the effect of the passive receiver NESz on the right panel the promising regions shrink to specular and quasi-orthogonal directions. Since it is very unlikely that SAOCOM-CS could perform measurement for θ_s>35-40°, the most promising range of scattering angles is for 25°<θ_s<35° and φ_s<80° (with the exception of a very narrow band in which the accuracy get worse).

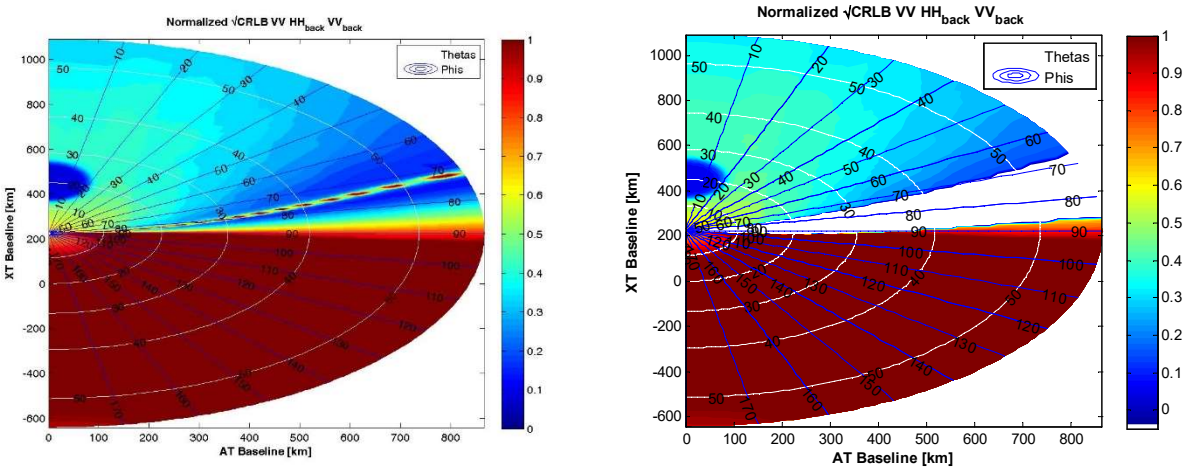

Figure 4-1: Maps of normalized CRLB for a bare soil as a function of the along-track (AT) and cross-track (XT) baselines. Zenith θs and azimuth φ_s scattering angles are reported in figure as contour plots. CRLB is obtained with a bistatic VV and two monostatic HH and VV measurements. Simulations were performed by considering a bistatic NESz=-25dB and a monostatic NESz=-30 dB (right) and without them (left). SMC is the retrieval parameter, sds is the noise parameter. The incidence angle is ϑ_i=20°, ACF=Exponential, L=12cm. σ° values below the NESz are represented in white.

In summary, the best bistatic configurations for soil moisture are Bistatic-2 and Specular. Bistatic-2 poses a problem of sensitivity as the expected signal is close to the receiver noise floor (i.e., small Neσ°). For this reason we cannot go too close to the exact 90° condition and we have to consider VV polarization and small incidence angles, conditions were the Bistatic-2 signal is slightly higher. Regarding the specular configuration the main drawback is the low resolution, as the radar is not able to discriminate in range. The mechanism that makes

Bistatic-2 the most effective for soil moisture retrieval is the higher sensitivity to the parameter. The mechanisms that makes the specular configuration effective for soil moisture retrieval is the opposite sensitivity to soil roughness exhibited by monostatic and specular observations. Simply speaking, if both monostatic and specular scattering increase we argue that soil moisture has increased, while an opposite trend at specular and backward directions indicates a variation in the soil roughness.

4.1.2 Crop biomass

The analysis of CRLB has been performed saturating the bistatic signal at -25dB, in order to take into account the reduced dynamic range of SAOCOM-CS with respect to SAOCOM that is assumed to perform the monostatic measurements with a NEσ^0=-30dB.

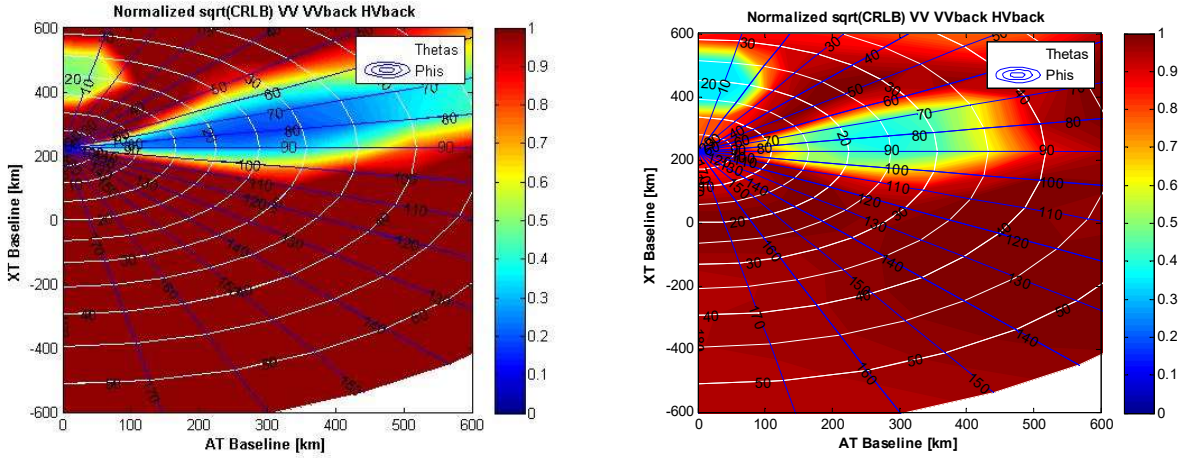

Figure 4-2: CRLB maps for a corn field, normalized to CRLB in the backscattering direction. Simulations were performed with IEM model (left) and with SSA2 model (right) for soil scattering. Plant height is the retrieval parameter, SMC is the noise parameter. The incidence angle is ϑ_i=20°.

In Figure 4-2, the square root of CRLB providing the crop biomass multistatic retrieval error, normalized to the backscatter case, is presented by a color coded map as function of cross-track and along-track baselines. Scattering angles, in azimuth and zenith, are also superimposed as black straight lines and white circles, respectively. The calculation of the CRLB in Figure 4-2 assumes a bistatic measurement at VV polarization together with the dual polarized (HV and VV) backscatter. Soil moisture is considered as the unknown nuisance parameter. Dark blue indicates the scattering angles where the lowest error, i.e., the best accuracy, is reached. The retrieval accuracy close to orthogonal directions is higher than the one pertaining to the monostatic dual acquisitions, and the retrieval error at orthogonal directions can be half of the error in the monostatic configuration (VV and HV). Similar configurations were proved to be effective also considering soil moisture as the parameter to be retrieved, and plant height as a nuisance parameter.

The reduced dynamic range implies a reduction of the sensitivity, whose overall effect is quite restrained in case of corn covered soil (with scattering vegetation), as opposed to bare soil where the noise floor limit is reached more often.

In conclusion, the bistatic geometric more effective for crop biomass retrieval based on the CRLB analysis is with an incidence angle θ_i ~20° (as small to prevent the noise floor

saturations) collecting VV polarization (less affected by the noise floor) with θ_s =25-35° and φ_s =70-80°. Another blue-green area in the maps is always observed around specular direction; this will be discussed later, as it is considered interesting specifically in the frame of forest monitoring.

4.1.3 Forest AGB and SMC strips (specular)

For vegetated targets, coherent soil scattering, attenuated by the above lying vegetation, represents the dominant contribution, so that attenuation turns out to be the main mechanism through which the specular response depends on biomass. In the specular direction, the incoherent contribution from vegetation volume is several dB's lower, whereas the coherent scattering has a decreasing trend with plant water content or biomass whose sensitivity is maintained even when tree biomass is very large.

Considering the effectiveness of Bistatic-2 configuration for crop monitoring, where a fair spatial resolution can be achieved by SAOCOM-CS, the specular configuration remains a powerful tool for quantitative assessment of forest Above Ground Biomass (AGB), in spite of the poor resolution and coverage. This kind of measurements can effectively integrate SAOCOM monostatic data and complement tomographic observations. Indeed, the latter are based on the reconstruction of the backscattering 3-D profile, while specular measurements are determined by the overall vegetation attenuation that can be evaluated quantitatively.

4.1.4 Anisotropic surfaces: a preliminary investigation

A bistatic radar could be useful for detecting the azimuth anisotropy of the earth surface. In order to preliminarily investigate this concept, we have considered a bare soil rough surface, whose incoherent bistatic scattering can be predicted by the AIEM model. Without considering coherent effects, which are beyond the scope of this work, it has been adopted an expression of the surface AutoCorrelation Function (ACF) with standard deviation σ, whose correlation lengths are different along the two Cartesian axes (respectively L_x and L_y).

Any rotation cannot be detected in backscattering since it affects in the same way the two polarizations. The potential of bistatic observations in this field was shown by the decrease of CRLB of soil moisture retrieval when anisotropy is unknown in almost all bistatic configurations. However the improvement is not significant for a set of bistatic angles which approximately correspond to an increase of AT baseline only. Then the Bistatic-1 configuration of SAOCOM-CS seems not to be much effective, although with an AT baseline of at least say 200 km we can notice some advantages.

Another way to look at the capability of a bistatic system to detect anisotropy was investigated for the sea surface. This case study has been investigate using the SSA2 model including the Elfouhaily sea wave spectra. The software package used for this investigation has been developed by Dr. Franco Fois and made available in the frame of a scientific cooperation. It is known that retrieving wind speed is not feasible from SAR without a knowledge of the wind direction coming from other sources. We used the CRLB tool to predict the wind speed retrieval accuracy of a multistatic radar combining VV measurements in monostatic and bistatic. The results are reported in Figure 4-3 both in the scattering direction and the AT and XT baseline coordinate domain. We can notice the high error in case of backscattering (XT=AT=0 or θ_s=20°, φ_s=180°) which goes down to around 4 m/sec

when bistatic angle is large. It is noticeable that we found a significant improvement also in Bistatic-1 configuration, provided that the AT baseline is long enough (at least 250 km).

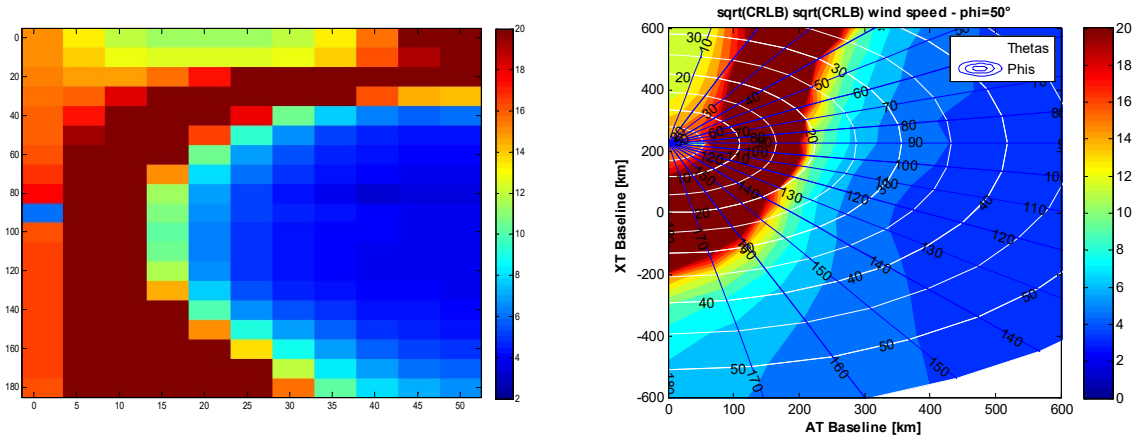

Figure 4-3: square root of the CRLB predicting the wind speed retrieval error standard deviation of a multistatic system in case wind direction is unknown. CRLB computation considers w=10 and 25 m/sec, ϕ=0° and 50°. Left panel is plotted in the zenith and scattering angle space, right panel is plotted in the XT and AT baseline space.

4.2 Land cover mapping

The model simulations performed for bare soil, forests and corn will were used to estimate the separability of these 3 classes in several feature spaces. The feature spaces that have been taken into account always include a monostatic measurement in order to evaluate the improvement in classification when bistatic measurements are available. Some results of the average class separability (expressed in dB) are reported in Figure 4-4. It can be observed that maximum separability can be obtained when a measurement at the orthogonal bistatic configuration is added to the monostatic measurement. The various scattering mechanisms contribute to the total scattering with different weights with respect to backscattering and give rise to different signal intensities than can allow achieving a better classification performance.

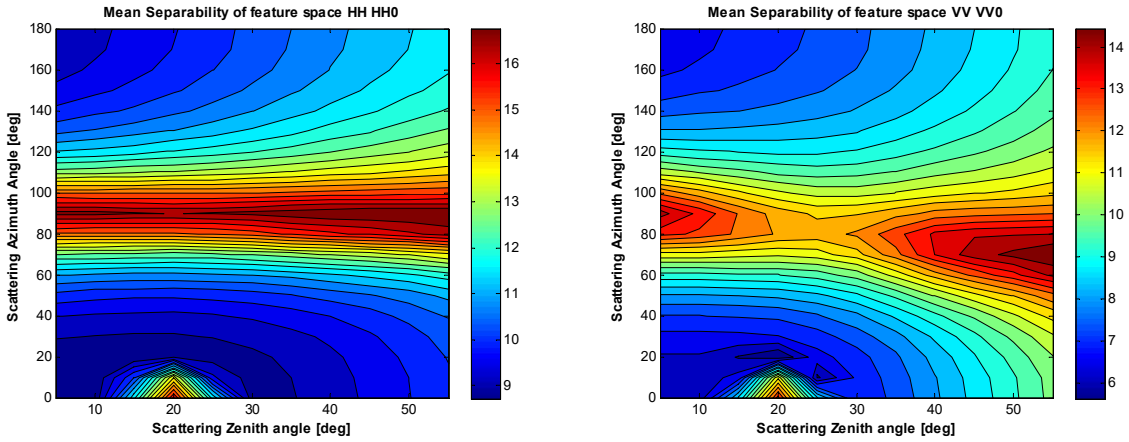

Figure 4-4: Maps of average class separability (in dB) for the 2-D feature spaces: Monostatic HH and Bistatic HH (top left); Monostatic VV and Bistatic VV (top right);

Note that an improvement of class separability is observed also in specular configuration, a case which is not of interest since the spatial resolution is not compatible with typical requirements of thematic map applications.

4.3 Multistatic image-like examples

The radiometric differences between land targets in bistatic configuration can be appreciated through images, also in comparison to the corresponding monostatic acquisitions, thus putting in evidence scattering directional properties. For this purpose, we pictured a fictitious scenario that has been used as a reference to create simulated *imagettes* with speckle. The land cover map includes 4 crops and 4 bare soil fields, two forest fields and a road.

The simulation of the *imagette* in monostatic and bistatic modes considers the most relevant image quality parameters that is radiometric resolution (i.e., number of looks) and geometric resolution. We assumed Level 1b products (the calibrated and geocoded images of radar backscatter) from SAOCOM and SAOCOM-CS projected onto the same geographical grid in order to analyze the multistatic dataset for target parameter retrieval, and thus with the same pixel size. Then the different spatial resolution translates into different number of looks of each pixel of the multistatic stack.

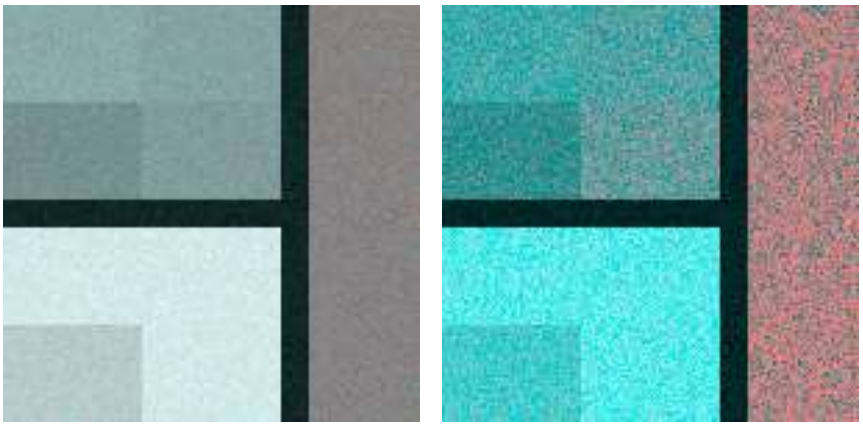

Figure 4-5: RGB color composite of monostatic HH (Red), monostatic VV (Green) and monostatic VV (Blue) on the left, and of bistatic VV (Red), monostatic VV (Green) and monostatic VV (Blue). Zenith incidence and scattering angle is 20° and bistatic azimuth angle is 80°. Stretching range is (-15 dB, 0 dB) for monostatic and (-30 dB, -5 dB) for bistatic.

Figure 4-5 compares the RGB composite of a simulated dual-pol monostatic (VV & HH) with that of a single-pol multistatic (VV backscatter and VV bistatic at 80 deg azimuth), with 20° of incidence angle and 100 and 56 looks for monostatic and bistatic images, respectively. When considering RGB composite of two channels, one is considered twice. It is possible to notice the higher color difference in the multistatic RGB composite, which indicates that the contrast between response from different targets in the scene are less correlated. In particular, the four crop fields can be better discriminated as the hue is more differentiated in the multistatic case.

4.4 Inversion results on simulated scenarios

We assessed retrieval algorithms on a simulated scenario formed by bare soil fields of which we want to measure soil moisture, or by crop fields where we want to measure the underneath soil moisture or the vegetation height. We have generated a scene composed of 100 squared fields, formed by 10x10 pixels each. We have also considered multitemporal observations, and in such case some parameters have been changed randomly from time to time, whereas other parameters have been kept constant. The algorithm was based on the inversion of the forward model (the one used to simulate the *imagettes*). With the availability of radar data with good temporal resolution, multitemporal approaches were considered as well.

4.4.1 Bare soil

The simulation of retrieval of soil moisture considered both the monotemporal and multitemporal algorithms. In order to predict the algorithm performances the retrieved soil parameters were compared to the ones used for image simulation, which represent the "truth" and standard score paramters were computed (i.e., Root Mean Square Difference and correlation coefficient). We can compare individual pixels, with retrieval performances affected by the residual speckle noise (i.e., speckle still present after the multilooking process). We can also assume to be able to single out each individual agriculture field, so that we can perform an averaging of the retrieved parameters, and then compare it with the field true values. In this case, the retrieval improves thanks to the additional averaging of 100 pixels within each 10x10 pixel field. The second (i.e., per-field) comparison could not represent a real situation, as it requires a detailed map of the area of interest distinguishing among different cultivations, not easily available in most cases.

The performances using multistatic data are better, as summarized in Table 4-1, even though the difference becomes almost irrelevant when we compare the case of multitemporal retrievals per-field. In this case both the multitemporal algorithm and the field averaging strongly mitigate the sensor noise effect on the retrieval, despite of the relatively low sensitivity to soil moisture and disturbing roughness effect on monostatic observations. In conclusion, the contribution of bistatic data is confirmed by the simulated experiment.

Table 4-1: Comparison of retrieval scores considering per-pixel and per-field test using monotemporal and multitemporal algorithms. Second and third column refer to monostatic (VV0 and HH0) and multistatic (VV0, HH0 and VV bistatic) observations, respectively. Each cell reports RMSE and correlation coefficient.

rms, corr	2 Pol monoST	3 Pol multiST	
MonoTemp	13.6%, 0.19	11.3%, 0.29	per pixel
MultiTemp	6.2%, 0.75	5.7%, 0.78	
MonoTemp	6.0%, 0.75	5.0%, 0.80	per field
MultiTemp	3.8%, 0.90	3.5%, 0.91	

4.4.2 Vegetated soil

For the case of vegetated surfaces, the plant height or the forest biomass has been retrieved applying a minimum squared difference monotemporal approach. The retrieved $\hat{h}, \hat{SMC}, \hat{\sigma}_z$ of each pixel correspond to the minimum squared difference between the pixel scattering coefficients and the simulated ones. In order to evaluate the accuracy of the retrieval, the difference between the retrieved values and the ground truth values of each pixel has been calculated. The RMSE, bias and error standard deviation have been finally computed for the multistatic configuration and compared against the best accuracy of the monostatic configurations.

In the following, the minimum difference algorithm has been applied using images acquired with the polarizations recommended by the CRLB and Chi-square accuracy predictors. This retrieval exercise has been carried out on two different data sets. The first one assumes that a large range of crop height can be found in the imaged fields. The second data set assumes that crops can have limited height. In both cases the accuracy of the height retrieval is higher when the orthogonal VV acquisition is added to the monostatic dual pol acquisition, as reported in Table 4-2,

Table 4-2: Comparison of retrieval performances based on Chi-squared and resulting from the simulated exercise with scene characterized by different plant height range.

		Dual pol mono VV0, HV0 StD of Height=55cm	Dual pol mono VV0, HV0 StD of Height=25cm
Backscattering accuracy std	Chi-squared	38 cm	22cm
	Simulations	25 cm	23 cm
Back+VV (θ_s~25°, φ_s~80°) std	Chi-squared	22 cm	17 cm
	Simulations	22 cm	18 cm

The possibility to retrieve soil moisture below a crop canopy has been also investigated. In this case, the orthogonal VV radar configuration has been coupled with the monostatic HH and VV acquisitions that are most sensitive to soil moisture parameters. The results show that the orthogonal image introduces information that help decoupling vegetation and soil effects, and makes the per-field retrieval error decreasing from 7.8 % to 5.5 % in the simulation.

4.4.3 Forest observed in Specular mode

Finally, a test on forest target has been performed. In the case of coherent scattering from forest, reflectivity is affected by soil surface roughness and is attenuated by the biomass overlying the soil. These effects are included in the equivalent reflectivity, which replaces the scattering coefficient in this configuration.

In specular configuration the range discrimination of the radar is not feasible, and then the spatial resolution is poor. Then, in the retrieval procedure, we coupled the backscattering from the different pixels in the field with a unique value of reflectivity provided by SAOCOM-CS in Specular direction. The specular signal is mostly coherent and so the concept of speckle noise does not apply. Nevertheless, we considered some noise affecting the reflectivity estimates. It might happen that assuming that the reflected signal comes from an individual homogeneous field is not reasonable, since mixed targets may contribute to the same

specular signal. This effect was taken into account by just increasing the error standard deviation.

In Figure 4-6, the forest biomass retrieval simulations for monostatatic acquisitions at VV and HV polarizations (red points) are compared to retrieval results obtained with the same monostatic acquisitions coupled with specular acquisition at VV polarization (blue points). The backscattering images were simulated with 100 looks, which corresponds to ~0.5 dB noise standard deviation, and a pixel resolution of about 100m. Each 10x10 pixel fields have therefore an area of 1000x1000 meters, comparable to the first Fresnel zone. Three different noise standard deviations of the specular reflectivity have been considered: about 0.5, 1.0 and 1.8 dB.

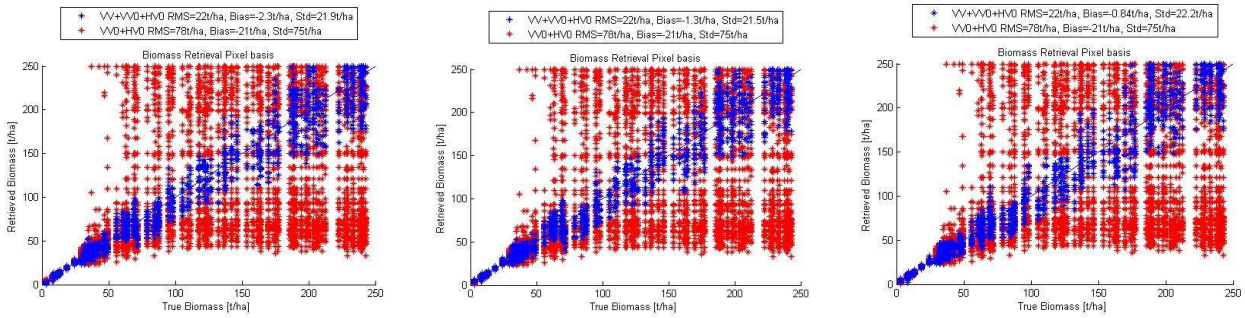

Figure 4-6: Forest biomass retrieval performance at pixel scale (time T_o) with 100 looks backscattering images (roughly 0.5 dB noise standard deviation, 100 m resolution) and noise standard deviation of specular reflectivity (about 1 km Fresnel zone) equal to ~0.5 dB (left), 1 dB (middle) and 1.8 dB (right).

The monostatic retrieval performance at pixel scale (red points) is very poor because of the well-known saturation problem. When adding the low resolution reflectivity in specular configuration even at pixel scale we get a significant improvement (blue points in Figure 4-6). The performances are always reasonable (about 20 cm) with respect to backscattering data only, regardless of noise.

Finally, an experiment was carried out simulating the retrieval of soil moisture under a forest plot with moderate unknown biomass and in presence of random variation of roughness. The backscattering data do not allow a reasonable retrieval of soil moisture in that condition, Including the low resolution specular data we get an improvement, although not very satisfactory yet, with RMSE going down to 6.8 % at pixels scale and to 3.8 % at field scale.

5 MULTISTATICA INTERFEROMETRY PERFORMANCE ASSESSMENT

5.1 3-D deformation performances

Monostatic radar interferometric measurements are only sensitive to the projection of the 3D deformation vector onto the radar line of sight (LOS). The sensitivity of the SAOCOM-CS system to the deformation components in East, North and Up direction was carried out for SAOCOM-CS viewing geometries in ascending and descending directions. Results are shown in Figure 5-1 as variance-covariance matrix of component errors normalized to variance of the Up component. The values should be multiplied by the variance of the Up component in

the case of the VC matrices and with that of LOS observations in case of standard deviations in Figure 5-1 right. The analysis shows that the North component still has the poorest sensitivity, but it is estimable. It also reveals that the Up component has large uncertainty dependence on the AT baseline length. Whereas for large baselines the Up component has a higher precision than the East one, for small baselines an ill-conditioning problem appears. If we have all four viewing geometries (ascending and descending, SAOCOM and SAOCOM-CS) the deformation estimation problem is solvable.

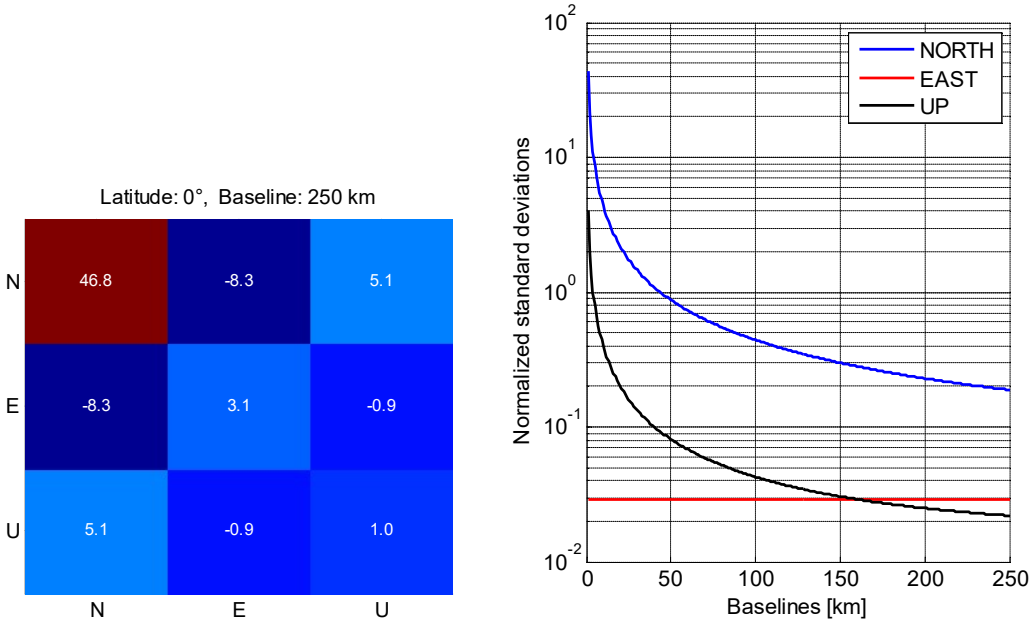

Figure 5-1. (left) Variance-covariance matrix (VC-matrix) of the North, East, Up components, at latitude 0° normalized to the Up component. (right) Standard deviation of North, East, Up components as a function of the AT baseline assuming unit variance for the phase observations.

A variability of the sensitivity with latitude is expected to be smaller (or comparable) than that of the AT baseline. The overall quality of the estimates is worsening with latitude.

5.2 InSAR Sensitivity to bistatic dihedral scattering

We investigated the sensitivity of bistatic InSAR systems to different SAOCOM-CS aperture settings and target orientation setups. The study focused on the co-polarimetric channels, and was specifically aimed at urban environments, where the most sensitive scatterers appear from dihedral-shaped objects. The bistatic polarimetric response of some representative dihedral reflectors at L-Band has been generated through a closed-form expression.

As a result, a simple preliminary proof of concept of the augmented target detection capabilities due to the joint monostatic-bistatic mission geometry was provided. We refer to Figure 5-2 to see that in the L-band case a 2 m reflector would be visible even with a 12° SAOCOM-CS bistatic aperture whereas a 2° aperture would be enough to apparently miss targets wider than 10 m.

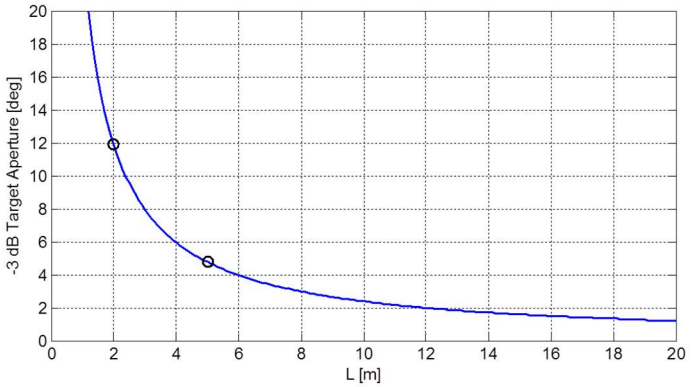

Figure 5-2. Azimuth visibility cone of dihedrals in L-Band configuration as a function of their width.

These considerations are however only based on clean amplitude responses without taking into account the effective target quality. The quality of a point target is defined by the ratio of the amplitude on the superimposed noise, rather than by its absolute amplitude. The noise includes both the thermal noise of the sensor and the clutter signal within the same resolution cell. Introducing the concept of target quality the analysis clearly conveys the message that a few degrees of bistatic aperture, 7-8°, would be enough to lead to a completely new set of double bounce scatterers with width larger than 5 m. The study also revealed that a long dihedral might ideally be bright enough to be visible by SAOCOM and SAOCOM-CS through its side-lobes. The relative gain in coherence attained by switching to the most convenient acquisition mode would then be lower than the one we could possibly have from a small and lower quality one. The occurrence of such phenomena in real case scenario is however deemed to be reduced by the natural irregularities in the target geometry and dielectric composition. In conclusion, this work provides a first proof of concept that the number of reliable scatterers can be augmented by using relatively broader azimuth angles. The choice of the optimal along-track baseline remains however of primary importance.

5.3 Optimal baseline final discussion

The choice of the baseline is not trivial. It was shown that enlarging the baseline helps achieving better deformation estimates, given the same target quality and distribution. It was however here elaborated how the latter target parameters change as well by increasing the baseline, most likely on a negative direction performance-wise. A few factors have been discussed whose relevance to the baseline choice can be schematically summarized as follows

Issue	Relevance	Notes
Target reflectivity	**High**	The loss of the ideal double bounce mechanism due to different incidence and scattering elevation has strong impact
Target noise (NESZ)	**Marginal**	Not relevant for Bistatic-1 mode
Target distribution	**Marginal**	Majority of applications will opt for high baseline and target diversity

Noise correlation	**Marginal** (long time series) to **Medium** (single interferograms)	A small performance increase could be achieved for small baseline. More quantitative assessments are needed

Out of the 4 addressed factors, 3 have been deemed as marginal. The weak impact of NESZ degradation was quantitatively demonstrated. The effects on the target distribution has also been regarded as not determinant on the baseline choice. The advantage of having a small baseline in asset monitoring applications is the possibility to illuminate the same target from two views, and attain 2D motion estimates on that. The quality of the target would however be hardly as high in both views and consequently the estimates accuracy. In general it is much more preferable to augment the target density, and thus to increase the baseline as far as possible. The third aspect concerns the correlation of the noise on the phase (LoS displacement) data. Such effect has a relevant impact especially on single interferograms, as long time series are supposed to effectively mitigate the atmospheric noise component.

In conclusion, the optimal trade-off is hypothesized to be mainly dependent on the reduction of the target reflectivity. Especially in urban scenarios, due to the loss of the double bounce mechanism for wide angles, the baseline should be calibrated as a function of the average target size. A baseline of 200 km would configure as the most effective choice in order not to lose targets with height equal or bigger than 5 m, and at the same time to mitigate the issue of saturation and side-lobe obstruction from strong scatterers. Future research efforts are expected to collect more quantitative evidence in such direction.

5.4 Interferometry processing

For 3D deformation vector estimation, four independent time series of single-look complex (SLC) data are required. The four stacks involve a SAOCOM monostatic time-series and a SAOCOM-CS time-series, using the illumination by SAOCOM. The same area of interest (AoI) should be covered by a descending as well as an ascending viewing geometry. We refer to these multiple geometries as multi-static InSAR. The time series should include at least 25 acquisitions to allow for estimating the atmospheric signal. Orbits and baselines should be controlled to minimize geometric decorrelation. Orbit knowledge (or better, location of the antenna phase center), should be on the sub-decimeter level in radial, across-track and along-track direction, enabling the geolocalization of targets (using an additional DEM) in a geodetic datum to the meter level. In order to estimate sufficient signal from slow-moving phenomena, e.g. tectonics, the total time span covered by the multi-static cycles should be at least three years.

L-band bi-static interferometry over land surfaces is of interest for several use cases. Considering such categories, the Bistatic-1 baseline configuration is the one of main interest. This follows the fact that Bistatic-1 allows a longer-term systematic time-series collection, which is of fundamental importance.

The steps of the multi-static InSAR processing chain leading to the final product outputs can be grouped in two categories:

1. The traditional InSAR mono-static processing algorithms, herewith recalled as multi-static pre-processig, which are independently applied to the SAOCOM and SAOCOM-CS interferometric stacks

2. The post-processing solutions conceived to combine the 4 different line-of-sight (LOS) displacements into the final product deliverable.

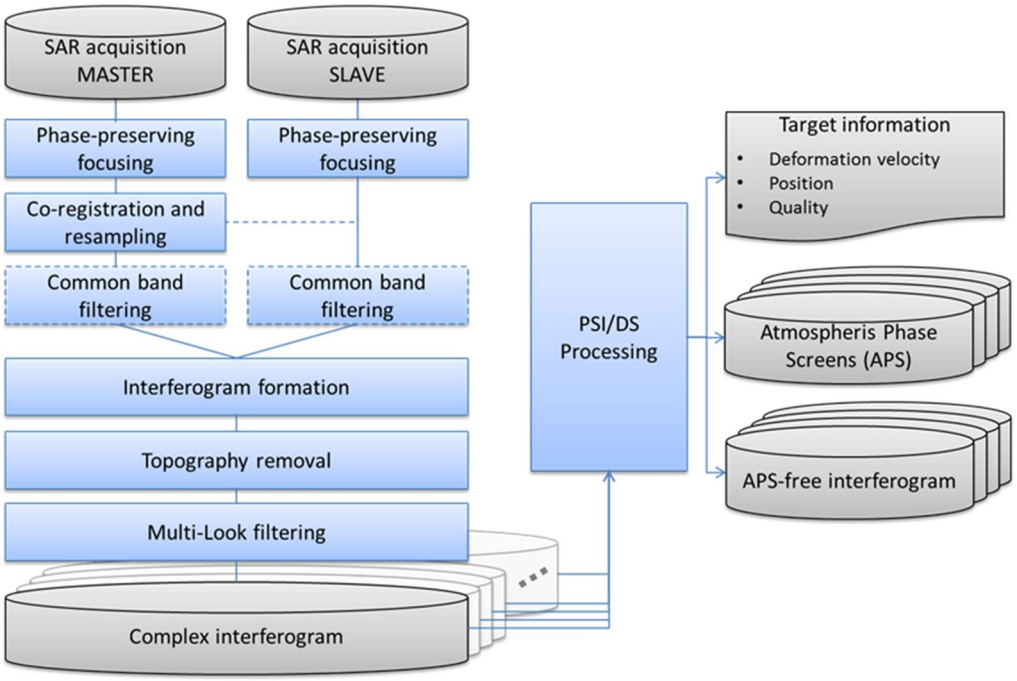

Figure 5-3. Mono-static InSAR processing chain.

6 SAOCOM-CS DEMONSTRATION PRODUCTS

6.1 Soil Moisture maps in Bistatic-2

Product summary. Around the orthogonal plane the sensitivity of bistatic scattering to soil moisture is higher than the one of backscatter (although the scattering coefficient itself presents lower absolute values) and this fact makes the improvement in the accuracy of the SMC retrieval possible. Then Table 6-1 summarizes the Level 2 soil moisture product.

Table 6-1- Soil Moisture L2 product in Bistatic-2

Mission Product	Product Description	Resolution	Product Coverage
SMC map (in Bistatic 2)	Volumetric soil moisture in m^3/m^3 in different roughness and crop vegetation conditions	1kmx1km (goal 250mx250m)	SAOCOM-CS swaths. Sites over Argentina and Australia.

Observational requirements. Requirements for the SMC estimation from multistatic acquisitions are:

- Acquisition geometry.

		θ_i (deg)	θ_s (deg)	φ_s (deg)
VV	Bistatic 2	20	25°-35°	70-80

- NESZ. In case of bare soil, the model simulations indicate a σ° dynamic range between -40 dB and 0 dB when receiving incoherent co-polarized signal close to 90° azimuth scattering angle. The required acquisition geometry was selected to limit the dynamic range from -25 to 0 dB.
- Geometrical Resolution. Goal is a value of 50 m of L1 image resolution, in order to achieve the required resolution of 1 km or better in the final SMC product by means of a multilooking processing.

6.2 Soil moisture strips in Specular

Product summary. In specular direction the effect of soil roughness is opposite with respect to that in backscattering. This enables a more accurate soil moisture retrieval in presence of variable and unknown roughness. The antenna synthesis is not feasible so only observations along a strip that is locus of specular reflection points are feasible.

Table 6-2- Soil Moisture L2 product in Specular

SMC strip (in Specular)	Volumetric soil moisture in m^3/m^3 in different roughness and crop vegetation conditions	1kmx1km, with specular points aligned along a strip parallel to the track	Strips of measurements along satellite track. Sites over Argentina and Australia.

Observational requirements. The requirements for the SMC estimation in specular scattering are:

- Acquisition geometry.

Polarizations	Phase	Acquisition geometry		
		θ_i (deg)	θ_s (deg)	φ_s (deg)
HH or VV	Specular	20	$\theta i \pm 5$	0 ± 10
		35	$\theta i \pm 5$	0 ± 5

- Polarizations. A dual polarization system is preferable.
- NESz. In case of bare soil, the model simulations indicate a required dynamic range between 10 dB and 30 dB (+30 dB is for very smooth soils, although within a sharp beam
- Geometrical Resolution. There isn't a requirement for the geometrical resolution. The resolution of 1 km comes out from the size of the first Fresnel zone (see section 7)

6.3 Crop biomass map in Bistatic-1

Product summary. VV polarization at ~90° of azimuth with respect to the incidence plane shows a double bounce effect between stems and ground, which is higher than double bounce effect at any polarization in backscatter configuration, as it is less screened by surface scattering. The same product resolution and coverage of the soil moisture map are considered (Table 6-1).

Observational requirements. They are the same specified for soil moisture maps.

6.3.1 *Biomass of dense forests in Specular mode*

Product summary. Specular measurements are expected to have the best performance as far as biomass sensitivity is concerned, since coherent scattering from the soil is gradually attenuated by forest biomass. Table 6-3 summarizes the Level 2 forest biomass product envisaged for SAOCOM-CS in specular configuration. Because of the low resolution issue, the specular products will be generated along lines parallel to the satellite ground track.

Table 6-3: Forest biomass Level 2 product in Specular configuration.

Mission Product	Product Description	Product Resolution	Product Coverage
AGB strip (in Specular)	Above ground biomass in ton/ha (or m^3/ha) of forest.	1kmx1km, with specular points aligned along a strip parallel to the track	Tropical forests, Amazonia and Congo basins

SAOCOM-CS acquisition requirements. They correspond to what required for the SMC strip product in Specular.

6.4 Deformation of the earth's surface

Product summary. The main use cases within this category are

1. tectonic deformation, related to earthquake hazards,
2. volcanic deformation, related to eruptive hazards,
3. slope deformation, related to landslide hazards,
4. subsidence, related to socio-economic impact and flooding, and
5. glacier deformation, related to ice dynamics and climate change.

A dataset of surface displacements in three dimensions is the main product of this use case. The product specifics are summarized in Table 6-4.

Table 6-4. Land surface interferometric L2 product in Bistatic-1 .

Mission product	Product Description	Product format	Product Coverage
Earth Surface Deformation map (in Bistatic-1)	Surface displacement (meters) in 3 dimensions (North,East,Up). This dataset could be converted in a (cumulative) displacement map, maps of deformation velocities, or derived products.	3D data cube (lat,lon,time) with the kinematic time series of each point in the adopted ground resolution (around 100m x 100m)	The product will be assessed over the tracks/frames covering selected test sites

Observational requirements. Assuming that the quality of the interferometric phases is approximately constant with the baseline, the accuracy in the 3D estimates has been shown to improve with increasing bistatic apertures.

6.5 Deformation of assets

Product summary. SAR interferometry represents a cost-effective technique to study and monitor the deformation of specific assets. These can refer to a wide range of anthropogenic structures, such as buildings, bridges, roads, dams and dikes among many others. The product outline is presented in Table 6-5.

Table 6-5. Asset deformation interferometric L2 product in Bistatic-1

Mission product	Product Description	Product format	Product Coverage
Asset Deformation map (in Bistatic-1)	Point/Target displacement (meters) in 3 dimensions (North,East,Up). This dataset could be converted in a (cumulative) displacement map, maps of deformation velocities, or derived products.	3D Point cloud (lat,lon,time) with the kinematic time series of each geo-located target.	The test phase will be conducted on ad-hoc sites with limited area.

Observational requirements. An along-track baseline of 200 km is deemed to provide a convenient balance among the contrasting analyzed aspects.

7 EXPERIMENTAL CAMPAIGNS

The definition of experimental campaigns is important for specifying mission requirements and confirming some of the theoretical findings obtained in this project. The gaps identified so far are the following:

- (Low) magnitude of sigma nought at 90° azimuth should be verified
- The higher sensitivity of backscattering to moisture around 90° azimuth should be verified and confirmed
- The double bounce enhancement of stems at 90° azimuth should be verified
- The anisotropy of surface models should also be verified
- Test focusing algorithms for large baselines and synchronization issues (different frequency bands could be considered)
- Verify bistatic response of buildings
- Verify 3D deformation performances

Different kinds of experimental activities can be planned according to different goals:

a. Indoor experiments by using anechoic chamber (EMSL) for model validation and specific small target observations
b. Outdoor ground based experiments by using
    i. Ground based scatterometers
    ii. Network analysers
    iii. Terrestrial radar
c. Aircraft experiments
    i. Using two aircrafts (in different configurations)
    ii. Using an aircraft and a ground-based bistatic receiver

d. Aircraft/satellite experiments
   i. Using the active signal from a satellite (ALOS/SAOCOM) and the receiver carried out by an aircraft
   ii. Using two satellites (ALOS/PALSAR, ALOS2/PALSAR2)
e. GNSS-R

Since not all the described experiments are really interesting for the selected applications, in the following table a list of the most performing experiments is presented along with the topic related to it, the main limitations and a final ranking in terms of priority.

Table 7-1. Ranking of priority of different experiments in view of SAOCOM-CS mission preparation

EXPERIMENT	GOAL	LIMITATIONS	PRIORITY
EMSL	-MODEL VALIDATION	-OBSERVATION OF SMALL TARGETS	MEDIUM
TERRESTRIAL RADAR	-3D or BUILDING RESPONSE	-NOT SIMULTANEOUSLY -FEW BISTATIC CONFIGURATIONS	MEDIUM/LOW
AIRCRAFTS (2)	-LARGE AREAS (SMC, CROPS & FORESTS) -RETRIEVAL VALIDATION -IMAGE QUALITY AND DEVELOPMENT/ASSESSMENT OF PROCESSING -INSAR VERIFICATIONS	-NOISE SOURCES: SYNCHRONIZATION, ORBITS, SENSORS, FOCUSING -EXPENSIVE AND TRICKY EXP.	MEDIUM (EXPENSIVE; it is expected to become HIGH at a later stage)
AIRCRAFT + TOWER	-CROPS, SMC (FOREST?) -MODEL VALIDATION	-LIMITED AREA DIMENSIONS -LOCATION AND TOWER HEIGHT	HIGH
AIRCRAFT+SATELLITE	-LARGE AREAS (SMC, CROPS & FORESTS) -MODEL VALIDATION	-NOISE SOURCES: SYNCHRONIZATION, ORBITS, SENSORS, FOCUSING -LOW FLEXIBILITY/ REPETITIVITY	LOW
SATELLITE (2) ALOS/PALSAR	-LARGE SCENES -3D BUILDING RESPONSE	-NO BISTATIC DATA. -SMALL AVAILABLE STACKS (FOR PSI) < 20 SCENES AND ONLY AVAILABLE IN ONE ORBIT DIRECTION (ASCENDING)	HIGH (LOW COST)
GNSS-R	FOREST BIOMASS	ONLY SPECULAR (3)	MEDIUM

8 CONCLUSIONS

This report demonstrates that SAOCOM-CS operational modes that foresee large baselines (Bistatic-1, Bistatic-2 and Specular) enable the generation of demonstration products; they should be assessed at least in limited areas on the earth during the mission. They are 3-dimensional deformation of the earth surface or assets by multistatic interferometry exploiting SAOCOM-CS data collected in Bistatic-1, soil moisture and crop biomass maps using multistatic radar scattering measurements exploiting data collected in Bistatic-2,

dense forest biomass or soil moisture measured along strips of data collected in Specular configuration. Other experimental objectives are also addressed, taking advantage from the high degree of innovation of the mission, which is expected by the scientific community to provide new opportunities to the advancement of the European EO capability. For instance, tomography of the atmosphere, sensing of the surface target anisotropy, mapping the sea wind vector at high resolution, observing underground features in arid zones and many other radio science experiments can become feasible during the SAOCOM-CS mission lifetime.

8.1 Intensity based products

Soil moisture content (SMC) will be measured by SAOCOM-CS with accuracy better than expected from monostatic radar, exploiting bistatic observations where sensitivity is higher and taking advantage from the capability of combined monostatic (from SAOCOM) and bistatic (i.e., multistatic) observations to better compensate for the disturbing effect of other parameters (i.e., soil roughness and vegetation cover). Indeed, notwithstanding the high revisit time (16 days), SAOCOM-CS will support the identification of the vegetation effect (crops) and calibrate the information on vegetation every other SMC estimation performed by SAOCOM. The improvement of the retrieval of soil moisture in Bistatic-2 configuration for bare soil, and in Specular configuration in vegetated conditions has been quantified by a simulated experiment that accounts for the main image quality parameters (radiometric and geometric resolutions of SAOCOM and SOACOM-CS). The same has been done for the retrieval of crop height in Bistatic-2 and forest biomass in specular mode. The experiment has provided realistic numbers in terms of expected retrieval accuracy associated to retrieval algorithms that may represent the baseline for future ground processing.

A novel possible application for exploiting the signal intensity has been also addressed in Bistatic-1 and Bistatic-2, that is the detection of the target anisotropy, such as soil roughness anisotropy or sea waves produced by the surface wind. In particular, some capability to infer high-resolution wind speed from a multistatic SAR has been demonstrated using SAOCOM-CS both in Bistatic-1 and Bistatic-2 configurations.

The test sites during in-orbit experiments will be selected where the presence of agricultural crops with fast growth cycle and changing roughness, due to erosive phenomena or agricultural practices, would make otherwise soil moisture retrieval very difficult. The sites shall be also well equipped to provide the necessary ground truth to prove the concept. Swamp forests were also identified for assessing the biomass retrieval in specular mode. However, an experimental verification of these findings is recommended during mission design and before the satellite launch. Very fundamental properties of bistatic scattering in the “90° degree azimuth” geometry shall be investigated by indoor experiments in an anechoich chamber. A very effective experiment, involving real targets (bare soil and crops) with high flexibility in terms of investigated bistatic geometry is that using an airborne transmitter and a ground receiver. As a final test and proof of the concept, an experiment with two aircrafts flying in formation to implement the most interesting configurations shall be carried out over agriculture areas, forests and urban areas (jointly with the InSAR oriented experiment). As for specular case, a synergy with the GNSS-R technique exists because of the commonality of frequency, which would suggest setting up common airborne experiments.

8.2 Interferometric products

We studied the potential of L-band bistatic interferometry for land applications, focusing on land deformation, asset deformation, and atmospheric integrated refractivity. We showed that a long along-track baseline is beneficial for use cases in these three application domains. The important premise is that such products are built upon the Bistatic-1 mode as it is the only configuration with long-term time-series acquisition capabilities. It was stressed that the number of images, in combination with the inherent quality of the monitored targets, represents the major discriminant on the product quality.

We also studied the dependency of coherent signals on dihedral reflection mechanisms. We concluded that an angular difference of more than 7 or 8 degrees would yield an almost completely different distribution of coherent samples over urban areas.

Finally, we were able to link the optimality of the baseline choice mainly to the increase of 3-D deformation accuracy for long baseline and to the loss of target quality with increasing bistatic angles. For large baselines the perfect double (or multiple) bounce mechanism is lost and consequently the target reflectivity. Whereas on one hand this would naturally help in solving the problem of "flashing" targets, on the other it would reduce the coherent signal strength for excessively large baselines. A 200 km baseline was hypothesized to guarantee an effective trade-off between sensitivity to 3D deformation and data quality, although further experimental investigations are needed considering that the optimal value may depend on the specific application (earth surface vs asset displacements).

A preliminary and inexpensive assessment of urban targets behaviour could be carried out by using existing satellite L-band monostatic radars. Terrestrial radars, thanks to the long-range capability, could also help investigating urban targets at least for few bistatic configurations. It is understood that an exhaustive answer to the open questions can only be provided by an airborne experiment (two aircrafts) to be carefully designed and prepared.

The basic ideas on the processing guidelines and on the eventual performance-limiting factors have been outlined for all the proposed multi-static interferometric products. The data from the different geometries are combined in a post-processing phase, recalled as 'multi-static post-processing', following the independent processing, within the so-called 'multi-static pre-processing' phase, of the 4 interferometers by means of well-known InSAR methods. This has been deemed as the most robust approach in regard of the fact that the coherence between the SAOCOM and the SAOCOM-CS imagery is lost for most of the targets at a baseline of 40 km.